

Lattice Preferred Orientation, Water Content, and Seismic Anisotropy of Orthopyroxene

Haemyeong Jung*, Munjae Park, Sejin Jung, Jaeseok Lee

Tectonophysics Laboratory, School of Earth and Environmental Sciences, Seoul National University, Seoul 151-747, Korea

ABSTRACT: Lattice preferred orientation (LPO) and seismic anisotropy of orthopyroxene (enstatite) in mantle xenoliths from Spitsbergen, Svalbard, near the Arctic, are studied. LPOs of enstatite were determined using electron backscattered diffraction (EBSD). We found four types of LPOs of orthopyroxene and defined them as type-AC, -AB, -BC, and -ABC. Type-AC LPO of orthopyroxene is defined as (100) plane aligned subparallel to foliation and [001] axis aligned subparallel to lineation. Type-AB LPO is defined as (100) plane aligned subparallel to foliation and [010] axis aligned subparallel to lineation. Type-BC LPO is defined as (010) plane aligned subparallel to foliation and [001] axis aligned subparallel to lineation. Type-ABC LPO is defined as both (100) and (010) planes aligned subparallel to foliation with a girdle distribution of both [100] and [010] axes normal to lineation and [001] axis aligned subparallel to lineation. We report for the first time the type-AB, -BC, and -ABC LPO of orthopyroxene. We found that the LPO pattern has a correlation with the content of orthopyroxene in the specimen. Nicolet 6700 FTIR (Fourier transformation infrared) study of enstatite showed that type-AC LPO was observed mostly in the samples of enstatite with low water content. It is found that the strength of the LPO of enstatite decreases with increasing water content and has a correlation with the strength of the LPO of olivine: the stronger the LPO of enstatite, the stronger the LPO of olivine. Seismic anisotropy of enstatite was smaller than that of olivine in the same specimen.

KEY WORDS: orthopyroxene, lattice preferred orientation, seismic anisotropy, mantle xenolith, Spitsbergen, FTIR.

INTRODUCTION

Orthopyroxene is the second most abundant mineral in the upper mantle and, together with olivine, is believed to be one of the major components of mantle

material (Ringwood, 1970). Since seismic anisotropy in the upper mantle is considered to be caused mainly by the lattice preferred orientation of olivine and orthopyroxene, understanding the LPOs of those minerals in nature is important. Lattice preferred orientation and seismic anisotropy are well known for olivine under both “dry” and “wet” conditions in experimental studies (Jung et al., 2009b, 2006; Katayama and Karato, 2006; Katayama et al., 2004; Jung and Karato, 2001; Bystricky et al., 2000; Zhang and Karato, 1995; Carter and Avé-Lallemant, 1970) and in many natural rocks (Kamei et al., 2010; Skemer et al., 2010, 2006; Jung, 2009; Jung et al., 2009a; Michibayashi et al., 2009; Tommasi et al., 2008; Michibayashi et al., 2006;

This study was supported by the Korea Meteorological Administration Research and Development Program (No. CATER 2008-5112).

*Corresponding author: hjung@snu.ac.kr

© China University of Geosciences and Springer-Verlag Berlin Heidelberg 2010

Manuscript received March 12, 2010.

Manuscript accepted May 21, 2010.

Katayama et al., 2005; Vauchez et al., 2005; Mizukami et al., 2004; Sawaguchi, 2004; Ben-Ismaïl and Mainprice, 1998; Nicolas and Christensen, 1987), whereas previous studies on the LPO of orthopyroxene and its seismic anisotropy have been limited (Soustelle et al., 2009; Hidas et al., 2007; Skemer et al., 2006; Vauchez et al., 2005; Christensen and Lundquist, 1982).

There are a few experimental studies on the plastic deformation of orthopyroxene. In experimentally deformed orthopyroxenes, (100)[001] slip has been characteristic (Green and Radcliffe, 1972; Raleigh, 1965). The deformation of enstatite (Raleigh et al., 1971) also showed that the slip of enstatite occurs at a pressure of 1.5 GPa and at temperatures of 1100–1300 °C at the strain rate of 10^{-3} – 10^{-6} s⁻¹, displaying a dominant slip system of enstatite (100)[001] and, less commonly, (100)[010]. Deformation experiments of polycrystalline enstatite aggregates from Webster, North Carolina, at $P=1$ GPa and a temperature range of 800–1300 °C (Ross and Nielsen, 1978) showed that the deformation of enstatite is dependent on both temperature and strain rate, and they observed the slip system (100)[001] throughout the whole P - T regime. They also reported a slip system (010)[001] at the uniaxial strains above 40%.

There have been some studies on the LPOs of orthopyroxene in natural rocks. According to Christensen and Lundquist (1982), the LPO of orthopyroxene (Opx) in naturally deformed rocks is exclusively controlled by only one slip system, namely, (100)[001]. Recent studies on the LPO of Opx in ultramafic rocks also suggest the same dominant slip system of (100)[001] for the deformation of Opx (Skemer et al., 2010, 2006; Soustelle et al., 2009; Tommasi et al., 2008; Hidas et al., 2007; Xu et al., 2006; Vauchez et al., 2005; Ishii and Sawaguchi, 2002; Vauchez and Garrido, 2001). However, most of previous studies on the LPO of Opx used a small number of data, and it is not clear yet if there are other LPO of Opx present and other slip systems operating for the deformation of Opx in nature.

Therefore, we studied the LPO of orthopyroxene (enstatite) in spinel lherzolite from Spitsbergen, Svalbard, with a large number of data for up to 215 grains. We found four different types of LPOs of enstatite and

defined them as type-AC, -AB, -BC, and -ABC. In the present paper, we report for the first time the type-AB, -BC, and -ABC LPO of Opx. To investigate the relationship between the LPO type, its strength and the presence of water in enstatite, samples were analyzed with a Nicolet 6700 FTIR microscope. Finally, the seismic anisotropy of enstatite was calculated and compared with the strength of the LPO of enstatite.

METHODS

Sample Descriptions

We studied ten mantle xenoliths from the Sverrefjell, Spitsbergen, Svalbard, which were collected during a field excursion in the summer of 2007. The study area is shown in Fig. 1, and detailed descriptions of the samples are given in a previous study (Jung et al., 2009a). We chose samples with well-developed foliation due to the compositional layering of clinopyroxene and spinel. Lineation of the sample was determined by grain shape analysis (Panozzo, 1984). Petrologically, the samples are spinel lherzolites. Olivine contents in the specimen are in the range of 40%–85%. Orthopyroxene contents are in the range of 10%–33%. Orthopyroxene is enstatite with a composition of $Wo_{0.9-1.4}En_{89.4-91.1}Fs_{7.8-9.5}$. Al_2O_3 and Cr_2O_3 concentrations have a range of 1.9 wt.%–4.1 wt.% and 0.2 wt.%–0.5 wt.%, respectively (Jung et al., 2009a). The equilibration temperature of the specimens was determined as $T=850$ – 1000 °C (Jung et al., 2009a) from the electron microprobe data using two-pyroxene thermometers (Brey and Köhler, 1990), and the pressures of the specimens were estimated as 7–11 kb by projecting the temperature estimates onto the geotherm for north-western Spitsbergen (Amundsen et al., 1987). The stresses of the specimens were previously determined as 10–20 MPa from the recrystallized grain-size of olivine (Jung et al., 2009a).

Determination of LPO

To determine the lattice preferred orientation (LPO) of the orthopyroxene, we used electron back-scattered diffraction (EBSD) patterns (Jung et al., 2006; Prior et al., 1999; Lloyd, 1987; Dingley, 1984). HKL's EBSD system attached to the JEOL JSM-6380 SEM at SEES in Seoul National University was used in this study. The LPO of enstatite was measured in

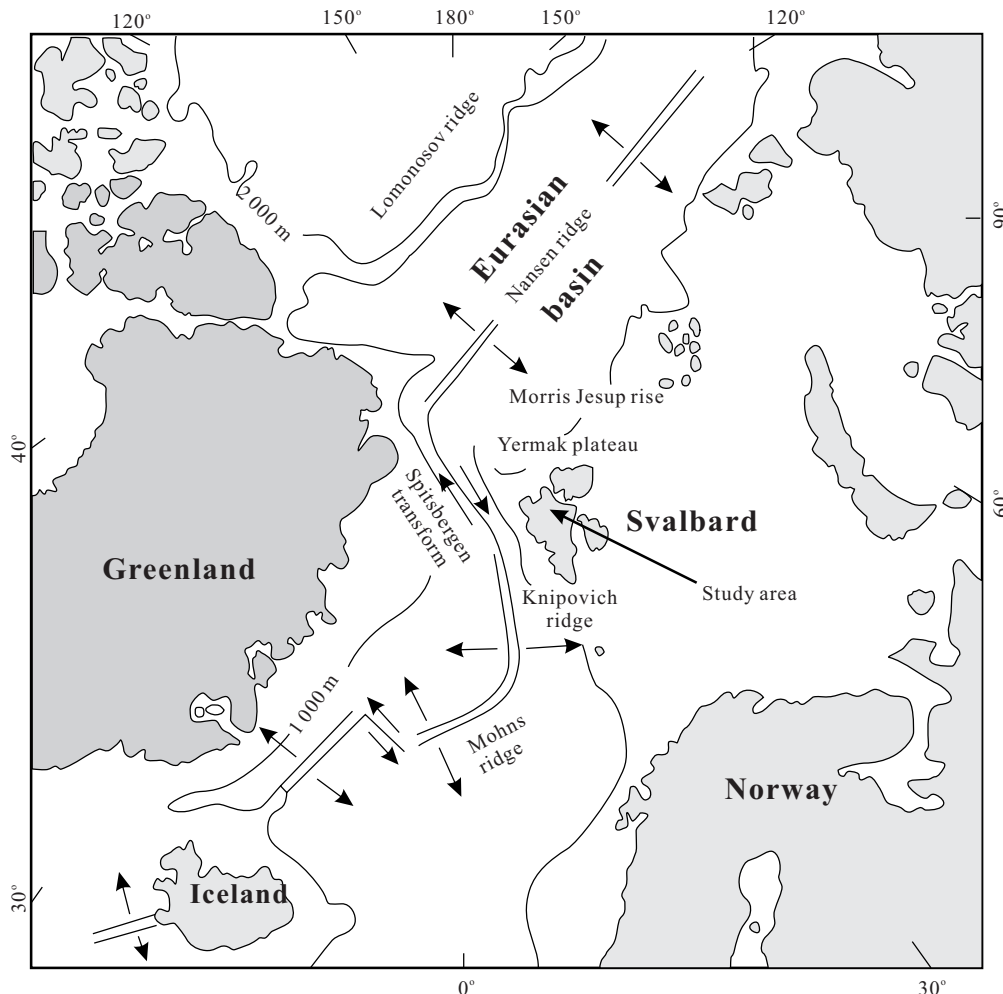


Figure 1. A schematic map of the study area of northern Spitsbergen, Svalbard, near the Arctic (after Ionov et al., 2002; Amundsen et al., 1987).

the X - Z plane of a thin section (X : lineation, Z : normal to foliation). Samples were polished using a 1- μm diamond paste, and then, to remove all of the surface damage, the specimens were polished using SYTON (0.06 μm colloidal silica) fluid for chemical-mechanical polishing (Lloyd, 1987). The specimens were coated with ~ 3 nm thick carbon to prevent charging in the SEM. The specimen surface was inclined at 70° to the incident beam. EBSD patterns were collected on the Nordlys II detector, where the experimental conditions were an accelerating voltage of 20 kV, a working distance of 15 mm, and a spot size of 60. All of the EBSD patterns were manually indexed to determine the orientation of the crystal accurately using HKL's Channel 5 software at the Tectonophysics Laboratory at School of Earth and Environmental Sciences, Seoul National University.

Determination of Water Content

Fourier transformation infrared (FTIR) spectroscopy was used to determine the hydroxyl concentration in orthopyroxene for each sample. All of the samples were polished on both sides down to 110–260 μm thick and were kept in an oven at 120°C for more than 24 h before an FTIR measurement was made. We used the Nicolet 6700 FTIR with a Continuum IR microscope at the Tectonophysics Laboratory at SEES in Seoul National University. We measured the water content within a single crystal using an IR beam size of $50\ \mu\text{m} \times 50\ \mu\text{m}$. N_2 gas was flushed through during the FTIR measurement to avoid measuring the moisture in the atmosphere. The measurements were carried out using an unpolarized light source, a KBr beam-splitter, and an MCT detector. A series of 128 scans was averaged for each spectrum with a resolution of $4\ \text{cm}^{-1}$.

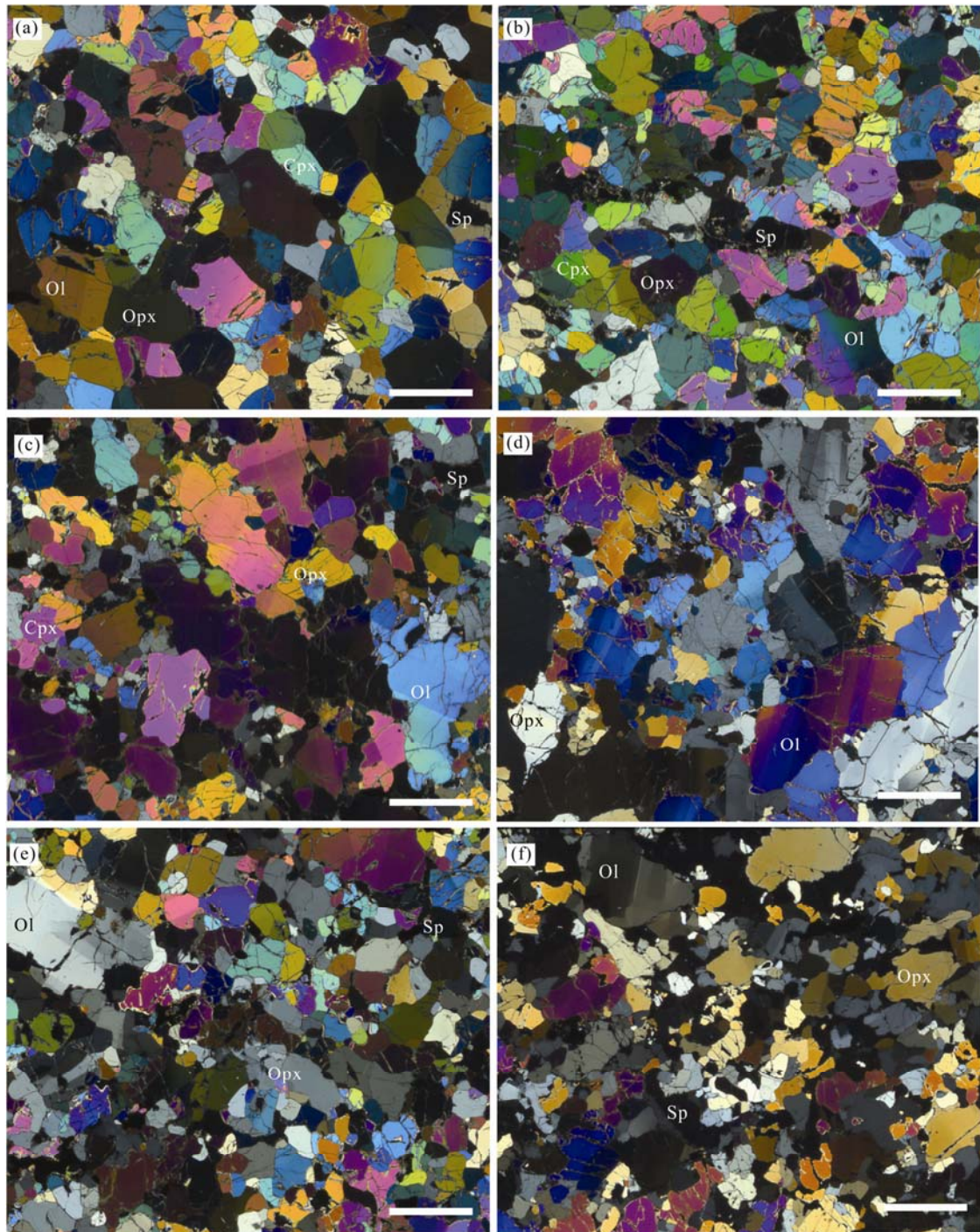


Figure 2. Optical photomicrographs of the analyzed peridotite samples. All images were taken under crossed polarized light. (a) Sample SVF-04 shows coarse equigranular texture. The microstructure is homogeneous. (b) Sample SVF-27 shows equigranular texture. Some grains show serrated grain boundaries and contain numerous inclusions. (c) Sample SVF-30 shows porphyroclastic texture. Grains are elongated up to aspect ratios of 3 : 1. Dynamically recrystallized grains are observed next to porphyroclasts. (d) Sample SVF-49. Porphyroclastic texture. Numerous kink bands are observed in olivine. Porphyroclasts are several millimeters in size and are locally elongated up to aspect ratios of 3 : 1. (e) Sample SVF-67 shows porphyroclastic texture. Undulose extinction is observed in the upper left corner. (f) Sample SVF-71. Porphyroclastic texture is shown with elongated grains up to aspect ratios of 4 : 1. The microstructure is relatively heterogeneous. Scale bars represent 2 mm for all the figures. Ol. Olivine; Opx. orthopyroxene (enstatite); Cpx. clinopyroxene (diopside); Sp. spinel.

RESULTS

We studied ten spinel peridotites from Sverrefjell, Spitsbergen, Svalbard, and the results are summarized in Table 1. The spinel peridotites show microstructures of equigranular texture (Figs. 2a, 2b) and porphyroclastic texture (Figs. 2c–2f) according to Mercier and Nicolas (1975). Kink bands and serrated grain boundaries are commonly observed in the specimens.

LPO of Enstatite

The LPOs of enstatite are shown in Fig. 3. Four types of LPOs of enstatite were observed. In the specimens SVF-27, -49, -66, and -70, the crystallographic [100] axis of enstatite was aligned subnormal to the foliation, and the [001] axis was aligned subparallel to the lineation, which is defined as type-AC. For the type-AC, the first and second capital letters (A and C) represent the slip plane (100) and slip direction [001], respectively. In the samples SVF-30, the crystallographic [010] axis was aligned subnormal to the foliation, and the [001] axis of enstatite was aligned subparallel to the lineation, which is defined as type-BC. For the type-BC, the first and second capital letters (B and C) represent the slip plane (010) and slip direction [001], respectively. Another sample SVF-05 shows a weak type-BC LPO. The [001] axis of enstatite is aligned subparallel to the lineation, but [010] axis is distributed weakly subnormal to the foliation. For the specimen SVF-04, the crystallographic [100] axis was aligned subnormal to the foliation, and the [010] axis was aligned subparallel to the lineation, which is defined as type-AB. In the specimen SVF-67, the crystallographic [010] axis is aligned subnormal to the foliation, the [001] axis is aligned subnormal to the lineation, and the [100] axis shows a weak LPO. Furthermore, for the sample SVF-71, the [001] axis of enstatite was aligned subparallel to the lineation, and both [100] and [010] axes were aligned mostly subnormal to the foliation with a girdle normal to the lineation, which is defined as type-ABC. The representative pole figures of enstatite are shown in Fig. 4a where different types of LPOs of enstatite are defined. Figure 4b shows LPO of olivine for the same specimen shown in Fig. 4a.

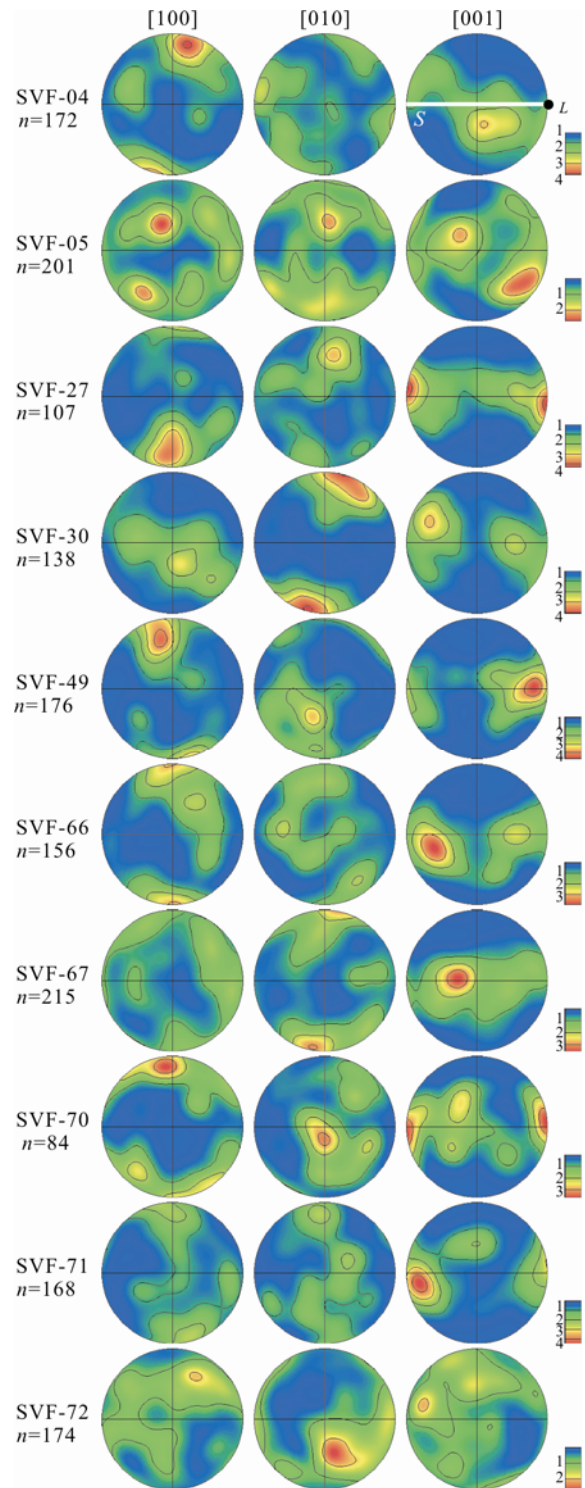


Figure 3. Pole figures of the crystallographic orientation of enstatite are presented in the upper hemisphere using an equal area projection. The color coding refers to the density of data points (the numbers in the legend correspond to the multiples of uniform distribution). A half scatter width of 30° was used. *S.* foliation; *L.* lineation; *n.* number of grains.

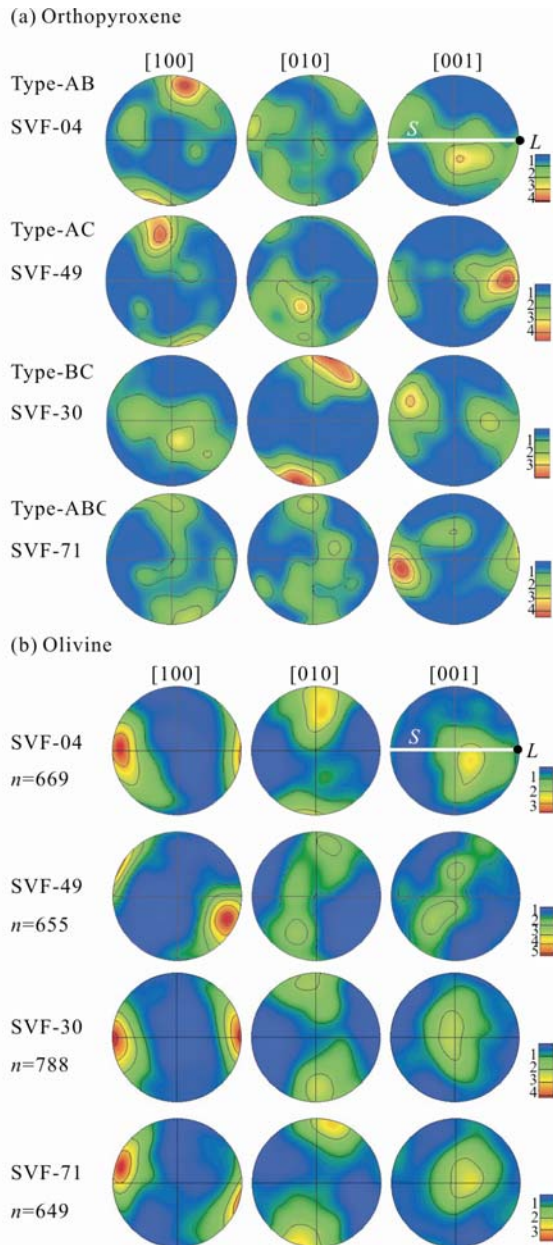


Figure 4. Pole figures of orthopyroxene (enstatite) and olivine. (a) Representative pole figures of enstatite. Type-AB: sample SVF-04, $n=172$; Type-AC: sample SVF-49, $n=176$; Type-BC: sample SVF-30, $n=138$; Type-ABC: sample SVF-71, $n=168$. (b) Pole figures of olivine (from Jung et al., 2009a) for the same sample shown in Fig. 4a. Legends are the same as in Fig. 3.

Inverse Pole Figures

Inverse pole figures are drawn for the specimens in the direction of lineation and normal to the foliation (Fig. 5). In the specimens SVF-27, -49, -66, and -70, crystallographic [100] axis was aligned nearly normal to the foliation, and crystallographic [001] axis was

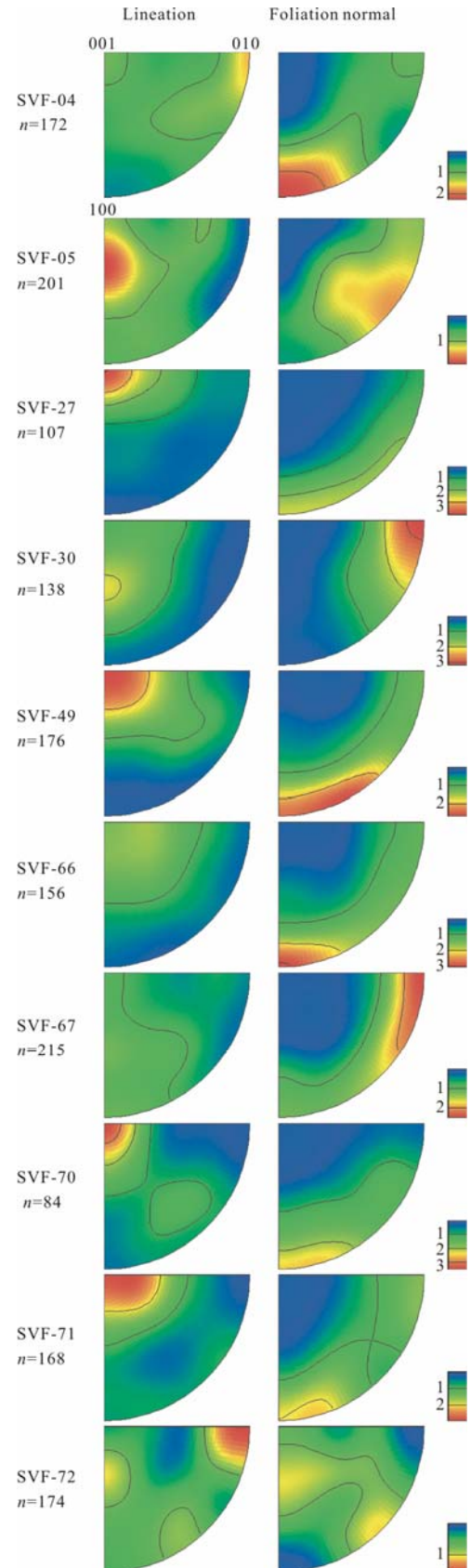


Figure 5. Inverse pole figures of enstatite. A half scatter width of 30° was used. The color coding refers to the density of the data points. n is the number of grains analyzed.

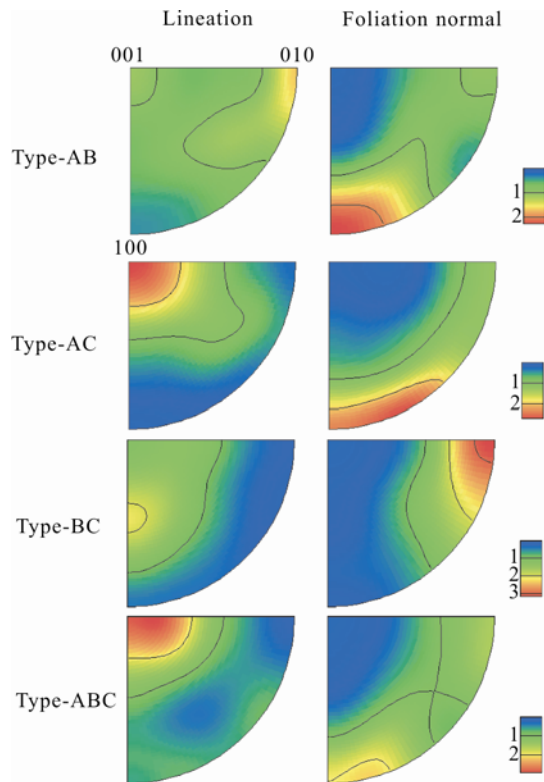


Figure 6. Representative inverse pole figures of enstatite. Type-AB: sample SVF-04, $n=172$; Type-AC: sample SVF-49, $n=176$; Type-BC: sample SVF-30, $n=138$; Type-ABC: sample SVF-71, $n=168$. Legends are the same as in Fig. 5.

aligned subparallel to the lineation, indicating a dominant slip system of (100)[001]. For the specimens SVF-05 and -30, crystallographic [010] axis was aligned subnormal to the foliation, and [001] axis was aligned subparallel to the lineation, indicating a dominant slip system of (010)[001]. For the specimen SVF-04, crystallographic [100] axis was aligned subnormal to the foliation, and [010] axis was aligned subparallel to the lineation, indicating a dominant slip system of (100)[010]. In the specimen SVF-67, crystallographic [010] axis is aligned subnormal to the foliation, and [100] axis is subparallel to the lineation, indicating a dominant slip system of (010)[100]. In addition, in the sample SVF-71, the [001] axis of enstatite was aligned subparallel to the lineation, and both [100] and [010] axes were aligned mostly subnormal to the foliation, indicating a combined slip system of (100)[001] and (010)[001]. Representative inverse pole figures of enstatite are shown in Fig. 6, where different types of inverse pole figures are de-

fined.

Water Content

Unpolarized FTIR spectra are presented in Fig. 7, which show a representative IR spectrum for each sample. A range of wave numbers 3100–4000 cm^{-1} is shown because the region is dominated by the stretching vibrations of O-H bonds (Paterson, 1982). The infrared beam is absorbed in the wave number range 3414 to 3595 cm^{-1} . The largest IR peak was observed at 3593, 3595, or 3597 cm^{-1} in most of the samples. Smaller IR peaks were also observed at the wave numbers of 3414, 3517, 3523, and 3567 cm^{-1} . These peaks show the presence of some amount of water in orthopyroxene (Grant et al., 2007a, b; Peslier et al., 2002; Bell et al., 1995; Skogby et al., 1990). The results of the FTIR study are summarized in Table 1. We measured the water contents of at least 10 grains of enstatite for each specimen and averaged them. The water content was estimated using a calibration (Paterson, 1982). The FTIR data showed that all of the enstatite samples contained some amount of water (350–1360 ppm H/Si). Water contents of olivine in the range of (40–160) ppm H/Si were previously reported from the same specimen (Jung et al., 2009a). Our results show that water content in the enstatite is much larger than that in olivine. Figure 8a shows that the water content of enstatite has a correlation with that of olivine. The more water there was in enstatite, the more water in olivine was observed. The water content of enstatite was also compared with the strength of the LPO (M -index) (Skemer et al., 2005), demonstrating that the strength of the LPO of enstatite decreases with increasing water content (Fig. 8b). In addition, we have found some correlation between the type of LPO and the water content of enstatite for the samples investigated. Most samples (SVF-49, -66, and -70) showing the type-AC LPO of enstatite contained a small amount of water (Table 1).

Seismic Anisotropy

Seismic velocity and seismic anisotropy were calculated using the orientation data from the EBSD analysis of orthopyroxene and a software (Mainprice, 1990), where we used the elastic constants of single crystal enstatite (Chai et al., 1997). Figure 9 shows the

results for the seismic velocity (V_P and V_S) and seismic anisotropy of shear waves in a pole figure. The P-wave (V_P) exhibited seismic anisotropy in the range of 1.8%–5.9%. The maximum anisotropy of the shear wave (AV_S) was in the range of 2.43%–3.97%. This is considerably weaker than the seismic anisotropy of

olivine (Jung et al., 2009a). Eight specimens showed that the polarization direction of the faster shear wave (V_{S1} polarization) was subparallel to the lineation (flow direction), while two samples (SVF-4 and -72) showed that the polarization direction of the faster shear wave deviated significantly from

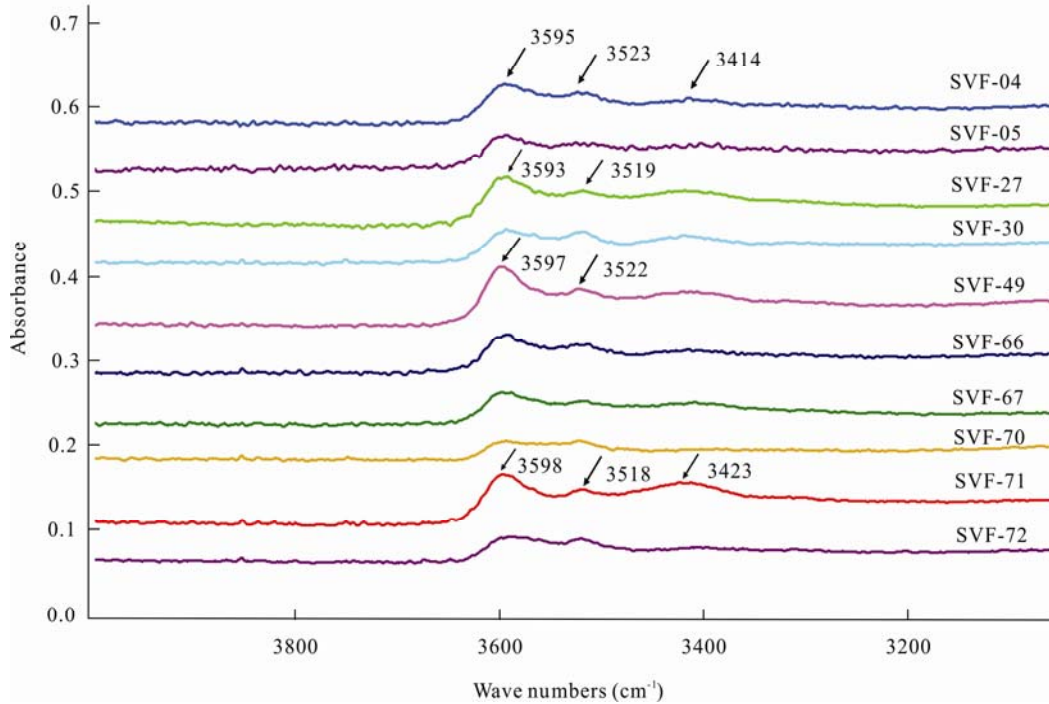


Figure 7. Unpolarized FTIR spectra of enstatite. A representative FTIR spectrum for each specimen is shown. An infrared beam size of $50\ \mu\text{m} \times 50\ \mu\text{m}$ was used in the transmission mode. Water content in enstatite was calculated using a calibration (Paterson, 1982). Water content and sample thickness are listed in Table 1.

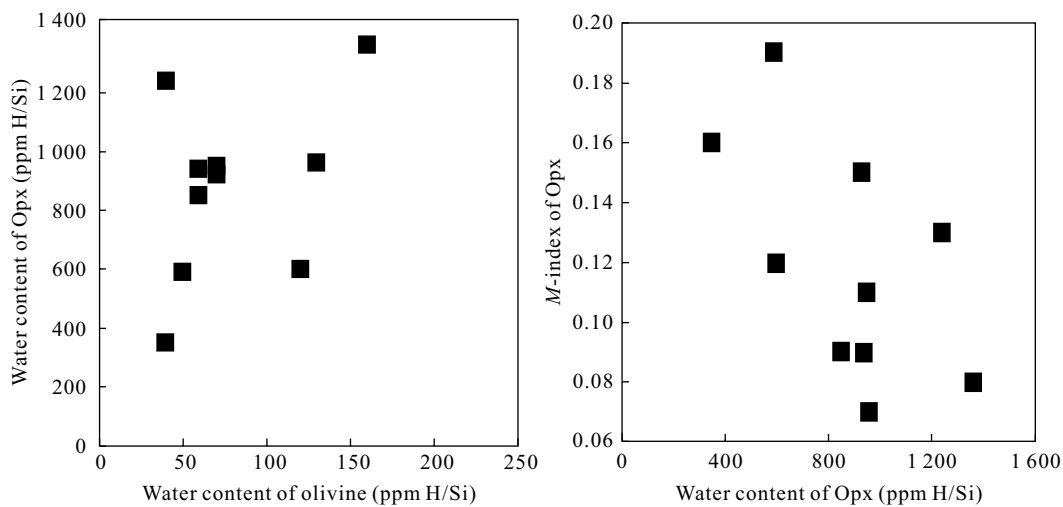


Figure 8. Water content of Opx (enstatite) compared with (a) water content of olivine and (b) LPO strength (M -index) of Opx in the same specimen. There is a trend that the water content of enstatite increases with increasing water content of olivine and M -index of Opx decreases with increasing water content of Opx.

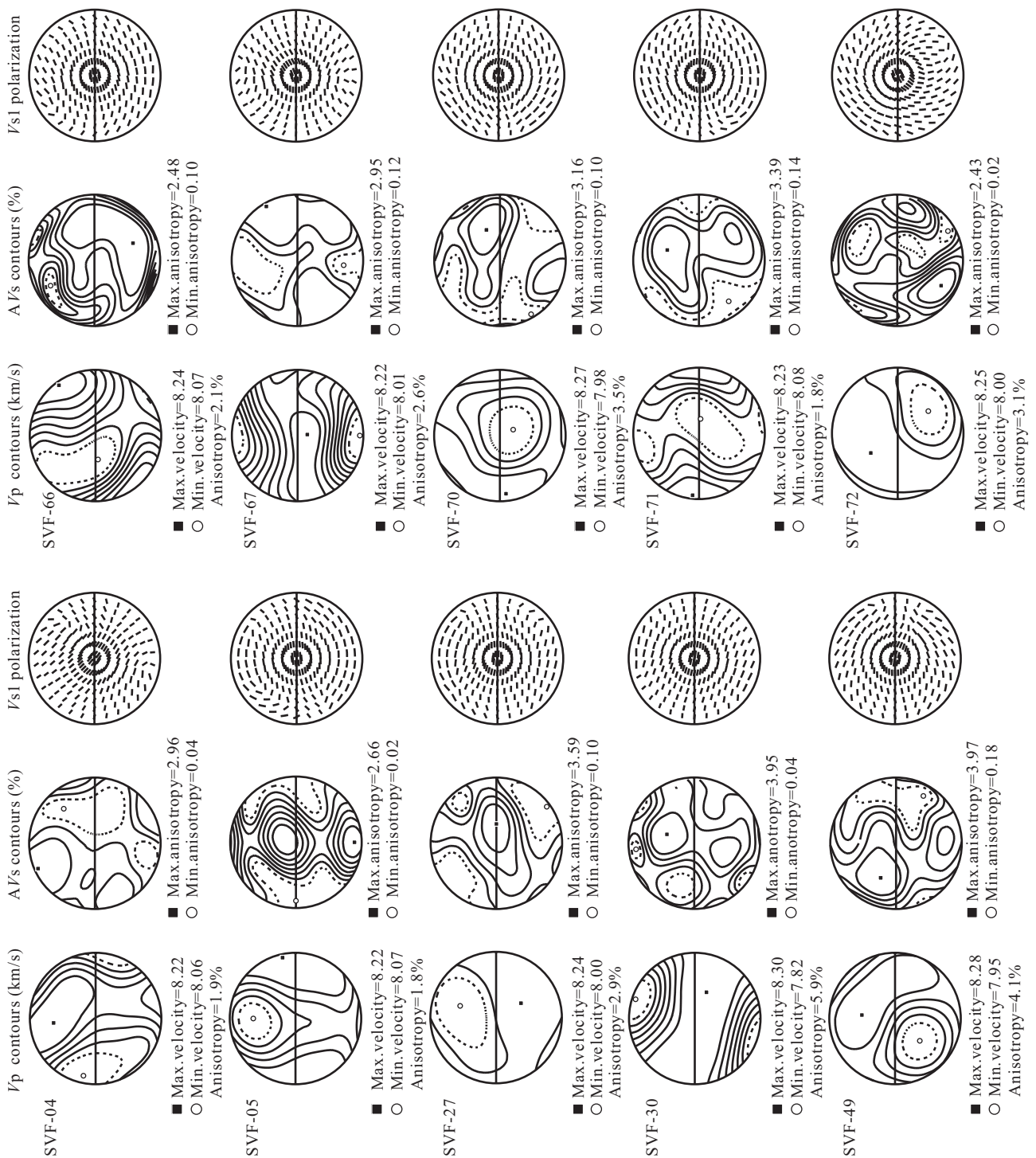


Figure 9. Seismic anisotropy corresponding to the LPO of enstatite. The east-west direction corresponds to the lineation (L), and the north-south corresponds to the foliation normal. Azimuthal anisotropy of P-waves (V_p) and polarization anisotropy of S-waves are shown (AV_s is a contour plot of the magnitude of shear wave polarization anisotropy and V_{s1} is a plot of the polarization direction of fast S-waves along different orientations of propagation).

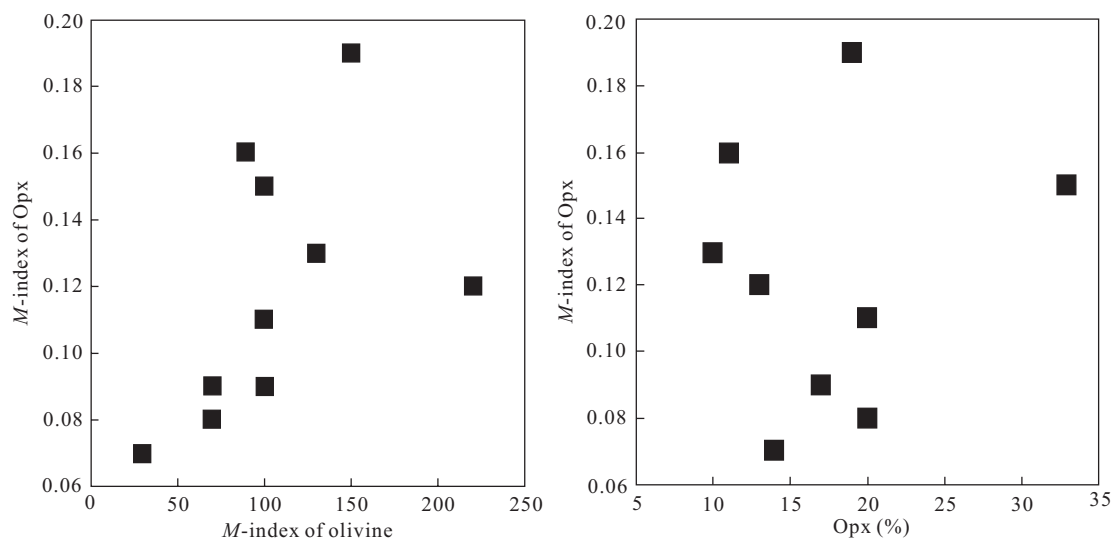


Figure 10. LPO strength (M -index) of Opx compared with (a) M -index of olivine and (b) amount of Opx (%) in each specimen. M -index of Opx increases in general with increasing M -index of olivine. However, there is no correlation observed in between the M -index of Opx and the amount of Opx.

Table 1 Sample description and results

Sample	Number of Opx (%) analyzed	Opx LPO ¹ type	Dominant slip system ² of Opx	M -index ³ of Opx	FTIR sample thickness (μm)	Opx. water content ⁴ (ppm H/Si)	Opx. Vp anisotropy ⁵ (%)	Max. AVs anisotropy ⁵ (%)
SVF-04	172 (20)	AB	(100)[010]	0.11	150	950	1.9	2.96
SVF-05	201 (17)	BC ⁶	(010)[001]	0.09	140	940	1.8	2.66
SVF-27	107 (10)	AC	(100)[001]	0.13	150	1240	2.9	3.59
SVF-30	138 (33)	BC	(010)[001]	0.15	120	930	5.9	3.95
SVF-49	176 (18)	AC	(100)[001]	0.19	250	590	4.1	3.97
SVF-66	114 (13)	AC	(100)[001]	0.12	160	600	2.1	2.48
SVF-67	215 (20)	-	(010)[100]	0.08	110	1360	2.6	2.95
SVF-70	84 (11)	AC	(100)[001]	0.16	260	350	3.5	3.16
SVF-71	168 (17)	ABC	(100,010)[001]	0.09	260	850	1.8	3.39
SVF-72	174 (14)	-	(1kl)[010]	0.07	110	960	3.1	2.43

¹Lattice preferred orientation (LPO) of orthopyroxene (Opx) was defined in this study based on the pole figure and dominant slip system. ²Dominant slip system of Opx was determined based on the inverse pole figure of Opx.

³ M -index is the misorientation index (Skemer et al., 2005) which shows the fabric strength of Opx.

⁴Water content of Opx was measured by Nicolet 6700 FTIR with a continuum IR microscope using a calibration of Paterson (1982). ⁵Seismic anisotropy of P- and S- wave (Vp and AVs) were calculated using the software (Mainprice, 1990). ⁶SVF-05 shows a weak type-BC.

the lineation (flow direction) (Fig. 9).

DISCUSSION

LPO of Enstatite

Four different types of LPOs of enstatite were observed in this study and we defined the LPOs of enstatite as type-AB, -AC, -BC, and -ABC where A, B, and C refer to 100, 010, and 001, respectively. The first capital letter refers to the slip plane and the second capital letter refers to slip direction. For example, type-AC is defined such that the slip plane is A (i.e., (100)) and slip direction is C (i.e., [001]), indicating a

slip system of (100)[001]. Type-ABC is defined such that the slip plane is both A and B (i.e., (100) and (010)) and slip direction is C (i.e., [001]). Among 10 specimens, four samples showed the type-AC LPO, two samples showed the type-BC LPO, while type-AB and -ABC LPO were seen in one sample each. Other two samples showed a complex LPO of enstatite. Four representative LPOs of enstatite are shown in Fig. 4a. Inverse pole figures corresponding to the LPOs are shown in Fig. 6. Type-AC LPO of enstatite has been well known and observed in previous studies of natural rocks (Soustelle et al., 2009; Tommasi et al., 2008;

Skemer et al., 2006; Xu et al., 2006; Ishii and Sawaguchi, 2002; Vauchez and Garrido, 2001; Mainprice et al., 2000; Christensen and Lundquist, 1982). Type-AB, -BC, and -ABC LPOs of enstatite are reported for the first time in this study. Dislocations with [010] as the Burgers vector have been occasionally observed in naturally deformed enstatite (Kohlstedt and Vander

Sande, 1973), in room temperature indentation of orthoenstatite (Vanduysen et al., 1985), and in a previous deformation experiment (Raleigh et al., 1971). Computer simulation also showed activation of the (100)[010] slip system in the deformation process of orthoenstatite (Jahn and Martonak, 2008).

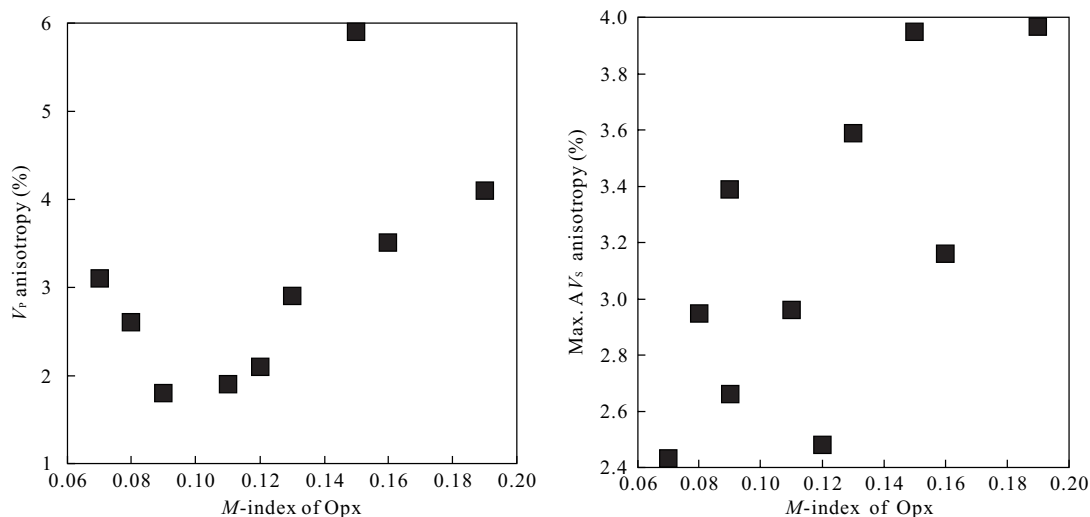


Figure 11. Seismic anisotropy compared with LPO (fabric) strength of Opx. (a) P-wave seismic anisotropy (V_p) is compared with fabric strength (M -index) of Opx. (b) Maximum S-wave seismic anisotropy (Max. AV_s (%)) is compared with M -index of Opx. Most samples show that both P- and S-wave anisotropy increase with increasing M -index of Opx.

LPO Pattern of Enstatite vs. Composition

We observed that the LPO pattern of enstatite has a correlation with the content of pyroxene in the specimen. Samples (SVF-27, -66, -70) showing type-AC LPO of enstatite (which has a dominant slip system of (100)[001]) contained a small portion of enstatite (10%–18%) and a large portion of olivine (50%–85%). On the other hand, samples (SVF-4, -30) showing the type-AB and -BC contained large portions of enstatite (20%–33%) in the specimens. It is not clear yet why this is so. We will need to investigate further to ascertain the mechanism which gives rise to four different types of LPO of enstatite.

Strength of LPO of enstatite versus olivine

The strength of LPO (M -index) of enstatite was calculated and shown in Table 1. The strength of the LPO of enstatite was compared with that of olivine in Fig. 10a. It is found that the M -index of Opx increases with increasing M -index of olivine. The M -index of

olivine was calculated in a previous study for the same sample (Jung et al., 2009a). It is also found that the M -index of Opx is not correlated to the amount of Opx in the specimen (Fig. 10b).

Seismic anisotropy versus the strength of LPO

Seismic anisotropy of the P-wave (V_p) was compared with the strength of the LPO of enstatite (M -index) and is shown in Fig. 11a. The P-wave seismic anisotropy (V_p) increases, in general, with increasing M -index of enstatite. Maximum shear wave anisotropy (AV_s) was also compared with the strength of the LPO of enstatite. As shown in Fig. 11b, the maximum anisotropy of the S-wave increases with the increasing M -index of enstatite. These results show that both P- and S-wave seismic anisotropy of enstatite increases with increasing fabric (LPO) strength, which is similar to that of olivine (Jung et al., 2009a).

CONCLUSIONS

We determined LPO of orthopyroxene (enstatite) in mantle xenoliths from Spitsbergen, Svalbard, near the Arctic, found four different types of LPOs of orthopyroxene, and defined them as type-AC, -AB, -BC, and -ABC (Fig. 4a). Four samples out of ten showed type-AC LPO of orthopyroxene, showing a dominant slip system of (100)[001]. In this study we are reporting for the first time type-AB, -BC, and -ABC LPOs of enstatite. We observed that the LPO pattern of enstatite has a correlation with the content of enstatite in the specimen. Type-AC LPO of enstatite was observed in the specimens which contain a small portion of enstatite (10%–18%), while type-AB, -BC and -ABC LPOs were observed in the specimens which contain a large portion of enstatite (17%–33%) (Table 1).

FTIR study showed that type-AC LPO was observed mostly in the samples of enstatite with low water content (Table 1). It is found that the strength of the LPO of enstatite decreases with increasing water content (Fig. 8b) and has a correlation with the strength of the LPO of olivine: the stronger the LPO of enstatite, the stronger the LPO of olivine. Seismic anisotropy of enstatite was calculated. P-wave anisotropy was in the range 1.8%–5.9% and S-wave anisotropy was in the range 2.4%–4.0%, which are weaker than those for olivine in the same specimen (Jung et al., 2009a).

ACKNOWLEDGEMENTS

This study was supported by the Korea Meteorological Administration Research and Development Program (No. CATER 2008-5112). We thank Dr. S H Choi for her help in chemical analysis and W Mo for providing assistance at the initial stage of the project. We wish to also thank two anonymous reviewers for critical and constructive reviews of the manuscript.

REFERENCES CITED

- Amundsen, H. E. F., Griffin, W. L., O'Reilly, S. Y., 1987. The Lower Crust and Upper Mantle beneath Northwestern Spitsbergen: Evidence from Xenoliths and Geophysics. *Tectonophysics*, 139(3–4): 169–185
- Bell, D. R., Ihinger, P. D., Rossman, G. R., 1995. Quantitative Analysis of Trace OH in Garnet and Pyroxenes. *American Mineralogist*, 80(5–6): 465–474
- Ben-Ismaïl, W., Mainprice, D., 1998. An Olivine Fabric Database: An Overview of Upper Mantle Fabrics and Seismic Anisotropy. *Tectonophysics*, 296(1–2): 145–157
- Brey, G. P., Köhler, T., 1990. Geothermobarometry in Four-Phase Lherzolites: II. New Thermobarometers, and Practical Assessment of Existing Thermobarometers. *Journal of Petrology*, 31(6): 1353–1378
- Bystricky, M., Kunze, K., Burlini, L., et al., 2000. High Shear Strain of Olivine Aggregates: Rheological and Seismic Consequences. *Science*, 290(5496): 1564–1567
- Carter, N. L., Avé-Lallemant, H. G., 1970. High Temperature Flow of Dunite and Peridotite. *Geological Society of America Bulletin*, 81(8): 2181–2202
- Chai, M., Brown, J. M., Slutsky, L. J., 1997. The Elastic Constants of an Aluminous Orthopyroxene to 12.5 GPa. *Journal of Geophysical Research—Solid Earth*, 102(B7): 14779–14785
- Christensen, N. I., Lundquist, S. M., 1982. Pyroxene Orientation within the Upper Mantle. *Geological Society of America Bulletin*, 93(4): 279–288
- Dingley, D. J., 1984. Diffraction from Sub-micron Areas Using Electron Backscattering in a Scanning Electron Microscope. *Scanning Electron Microscopy*, 2: 569–575
- Grant, K., Ingrin, J., Lorand, J. P., et al., 2007a. Water Partitioning between Mantle Minerals from Peridotite Xenoliths. *Contributions to Mineralogy and Petrology*, 154(1): 15–34
- Grant, K. J., Kohn, S. C., Brooker, R. A., 2007b. The Partitioning of Water between Olivine, Orthopyroxene and Melt Synthesised in the System Albite-Forsterite-H₂O. *Earth and Planetary Science Letters*, 260(1–2): 227–241
- Green, H. W., Radcliffe, S. V., 1972. Deformation Processes in the Upper Mantle. *Geophysical Monograph*, 16: 139–156
- Hidas, K., Falus, G., Szabo, C., et al., 2007. Geodynamic Implications of Flattened Tabular Equigranular Textured Peridotites from the Bakony-Balaton Highland Volcanic Field (Western Hungary). *Journal of Geodynamics*, 43(4–5): 484–503
- Ionov, D. A., Bodinier, J. L., Mukasa, S. B., et al., 2002. Mechanisms and Sources of Mantle Metasomatism: Major and Trace Element Compositions of Peridotite Xenoliths from Spitsbergen in the Context of Numerical Modelling. *Journal of Petrology*, 43(12): 2219–2259
- Ishii, K., Sawaguchi, T., 2002. Lattice- and Shape-Preferred Orientation of Orthopyroxene Porphyroclasts in Peridotites: An Application of Two-Dimensional Numerical

- Modeling. *Journal of Structural Geology*, 24(3): 517–530
- Jahn, S., Martonak, R., 2008. Plastic Deformation of Orthoenstatite and the Ortho- to High-Pressure Clinoenstatite Transition: A Metadynamics Simulation Study. *Physics and Chemistry of Minerals*, 35(1): 17–23
- Jung, H., 2009. Deformation Fabrics of Olivine in Val Malenco Peridotite Found in Italy and Implications for the Seismic Anisotropy in the Upper Mantle. *Lithos*, 109(3–4): 341–349
- Jung, H., Karato, S. I., 2001. Water-Induced Fabric Transitions in Olivine. *Science*, 293(5534): 1460–1463
- Jung, H., Katayama, I., Jiang, Z., et al., 2006. Effect of Water and Stress on the Lattice-Preferred Orientation of Olivine. *Tectonophysics*, 421(1–2): 1–22
- Jung, H., Mo, W., Choi, S. H., 2009a. Deformation Microstructures of Olivine in Peridotite from Spitsbergen, Svalbard and Implications for Seismic Anisotropy. *Journal of Metamorphic Geology*, 27(9): 707–720
- Jung, H., Mo, W., Green, H. W., 2009b. Upper Mantle Seismic Anisotropy Resulting from Pressure-Induced Slip Transition in Olivine. *Nature Geoscience*, 2(1): 73–77
- Kamei, A., Obata, M., Michibayashi, K., et al., 2010. Two Contrasting Fabric Patterns of Olivine Observed in Garnet and Spinel Peridotite from a Mantle-Derived Ultramafic Mass Enclosed in Felsic Granulite, the Moldanubian Zone, Czech Republic. *Journal of Petrology*, 51(1–2): 101–123
- Katayama, I., Jung, H., Karato, S. I., 2004. New Type of Olivine Fabric from Deformation Experiments at Modest Water Content and Low Stress. *Geology*, 32(12): 1045–1048
- Katayama, I., Karato, S. I., 2006. Effect of Temperature on the B- to C-Type Olivine Fabric Transition and Implication for Flow Pattern in Subduction Zones. *Physics of the Earth and Planetary Interiors*, 157(1–2): 33–45
- Katayama, I., Karato, S. I., Brandon, M., 2005. Evidence of High Water Content in the Deep Upper Mantle Inferred from Deformation Microstructures. *Geology*, 33(7): 613–616
- Kohlstedt, D. L., Vander-Sande, J. B., 1973. Transmission Electron Microscopy Investigation of Defect Microstructure of Four Natural Orthopyroxenes. *Contributions to Mineralogy and Petrology*, 42(2): 169–180
- Lloyd, G. E., 1987. Atomic Number and Crystallographic Contrast Images with the SEM: A Review of Backscattered Electron Techniques. *Mineralogical Magazine*, 51(359): 3–19
- Mainprice, D., 1990. A Fortran Program to Calculate Seismic Anisotropy from the Lattice Preferred Orientation of Minerals. *Computers & Geosciences*, 16(3): 385–393
- Mainprice, D., Barruol, G., Ismail, W. B., 2000. The Seismic Anisotropy of the Earth's Mantle from Single Crystal to Polycrystal. *Geophysical Monograph*, 117: 237–264
- Mercier, J. C., Nicolas, A., 1975. Textures and Fabrics of Upper-Mantle Peridotites as Illustrated by Xenoliths from Basalts. *Journal of Petrology*, 16(2): 454–487
- Michibayashi, K., Ina, T., Kanagawa, K., 2006. The Effect of Dynamic Recrystallization on Olivine Fabric and Seismic Anisotropy: Insight from a Ductile Shear Zone, Oman Ophiolite. *Earth and Planetary Science Letters*, 244(3–4): 695–708
- Michibayashi, K., Oohara, T., Satsukawa, T., et al., 2009. Rock Seismic Anisotropy of the Low-Velocity Zone beneath the Volcanic Front in the Mantle Wedge. *Geophysical Research Letters*, 36
- Mizukami, T., Wallis, S. R., Yamamoto, J., 2004. Natural Examples of Olivine Lattice Preferred Orientation Patterns with a Flow Normal *a*-Axis Maximum. *Nature*, 427(6973): 432–436
- Nicolas, A., Christensen, N. I., 1987. Formation of Anisotropy in Upper Mantle Peridotite: A Review. In: Fuchs, K., Froidevaux, C., eds., *Composition, Structure and Dynamics of the Lithosphere-Asthenosphere System*. Geodyn. AGU, Washington D.C.: 111–123
- Panozzo, R. H., 1984. Two-Dimensional Strain from the Orientation of Lines in a Plan. *Journal of Structural Geology*, 6(1–2): 215–221
- Paterson, M. S., 1982. The Determination of Hydroxyl by Infrared Absorption in Quartz, Silicate Glasses and Similar Materials. *Bull. Mineral.*, 105(1): 20–29
- Peslier, A. H., Luhr, J. F., Post, J., 2002. Low Water Contents in Pyroxenes from Spinel-Peridotites of the Oxidized, Sub-arc Mantle Wedge. *Earth and Planetary Science Letters*, 201(1): 69–86
- Prior, D. J., Boyle, A. P., Brenker, F., et al., 1999. The Application of Electron Backscatter Diffraction and Orientation Contrast Imaging in the SEM to Textural Problems in Rocks. *American Mineralogist*, 84(11–12): 1741–1759
- Raleigh, C. B., 1965. Glide Mechanism in Experimentally Deformed Minerals. *Science*, 150(3697): 339–341
- Raleigh, C. B., Kirby, S. H., Carter, N. L., et al., 1971. Slip and the Clinoenstatite Transformation as Competing Rate Processes in Enstatite. *Journal of Geophysical Research*,

- 76(17): 4011–4022
- Ringwood, A. E., 1970. Phase Transformations and the Constitution of the Mantle. *Physics of the Earth and Planetary Interiors*, 3: 109–155
- Ross, J. V., Nielsen, K. C., 1978. High-Temperature Flow of Wet Polycrystalline Enstatite. *Tectonophysics*, 44(1–4): 233–261
- Sawaguchi, T., 2004. Deformation History and Exhumation Process of the Horoman Peridotite Complex, Hokkaido, Japan. *Tectonophysics*, 379(1–4): 109–126
- Skemer, P., Katayama, I., Jiang, Z. T., et al., 2005. The Misorientation Index: Development of a New Method for Calculating the Strength of Lattice-Preferred Orientation. *Tectonophysics*, 411(1–4): 157–167
- Skemer, P., Katayama, I., Karato, S. I., 2006. Deformation Fabrics of the Cima di Gagnone Peridotite Massif, Central Alps, Switzerland: Evidence of Deformation at Low Temperatures in the Presence of Water. *Contributions to Mineralogy and Petrology*, 152(1): 43–51
- Skemer, P., Warren, J. M., Kelemen, P. B., et al., 2010. Microstructural and Rheological Evolution of a Mantle Shear Zone. *Journal of Petrology*, 51(1–2): 43–53
- Skogby, H., Bell, D. R., Rossman, G. R., 1990. Hydroxide in Pyroxene-Variations in the Natural Environment. *American Mineralogist*, 75(7–8): 764–774
- Soustelle, V., Tommasi, A., Demouchy, S., et al., 2009. Deformation and Fluid-Rock Interaction in the Supra-Subduction Mantle: Microstructures and Water Contents in Peridotite Xenoliths from the Avacha Volcano, Kamchatka. *Journal of Petrology*, 51(1–2): 363–394
- Tommasi, A., Vauchez, A., Ionov, D. A., 2008. Deformation, Static Recrystallization, and Reactive Melt Transport in Shallow Subcontinental Mantle Xenoliths (Tok Cenozoic Volcanic Field, SE Siberia). *Earth and Planetary Science Letters*, 272(1–2): 65–77
- Vanduysen, J. C., Doukhan, N., Doukhan, J. C., 1985. Transmission Electron Microscope Study of Dislocations in Ortho-Pyroxene (Mg, Fe)₂Si₂O₆. *Physics and Chemistry of Minerals*, 12(1): 39–44
- Vauchez, A., Dineur, F., Rudnick, R., 2005. Microstructure, Texture and Seismic Anisotropy of the Lithospheric Mantle above a Mantle Plume: Insights from the Labait Volcano Xenoliths (Tanzania). *Earth and Planetary Science Letters*, 232(3–4): 295–314
- Vauchez, A., Garrido, C. J., 2001. Seismic Properties of an Asthenospherized Lithospheric Mantle: Constraints from Lattice Preferred Orientations in Peridotite from the Ronda Massif. *Earth and Planetary Science Letters*, 192(2): 235–249
- Xu, Z. Q., Wang, Q., Ji, S. C., et al., 2006. Petrofabrics and Seismic Properties of Garnet Peridotite from the UHP Sulu Terrane (China): Implications for Olivine Deformation Mechanism in a Cold and Dry Subducting Continental Slab. *Tectonophysics*, 421(1–2): 111–127
- Zhang, S. Q., Karato, S. I., 1995. Lattice Preferred Orientation of Olivine Aggregates Deformed in Simple Shear. *Nature*, 375(6534): 774–777